THE ASTROPHYSICAL JOURNAL, 413:531–541, 1993 August 20

THE DUSTY EMISSION FILAMENTS OF M87[1]

W. B. SPARKS
Space Telescope Science Institute, 3700 San Martin Drive, Baltimore, MD 21218
H. C. FORD[2]
Johns Hopkins University and Space Telescope Science Institute
AND
A. L. KINNEY[2]
Space Telescope Science Institute, 3700 San Martin Drive, Baltimore, MD 21218
Received 1992 October 21; accepted 1993 February 24

ABSTRACT

Emission-line and continuum images show that the Hα + [N II] filaments in M87 have a double stranded or ribbon-like morphology and that they are dusty. Spectroscopy of the filaments shows smoothly varying velocities within individual features. The innermost filaments are blueshifted with respect to systemic velocity. The presence of *absorption* associated with the emission filaments and alignment with the radio/optical jet suggests that this is foreground material, in which case it is flowing *out* from the nucleus rather than falling in. Conversely, line emitting gas associated with the more distant radio lobe, as deduced from Faraday rotation observations, appears to be background material, in which case it is *infalling* and not outflowing.

By assuming pressure equilibrium between the filaments and coronal X-ray emitting gas, we estimate a *high* dust-to-ionized gas ratio, indicating that either the filaments are very dusty or there is a significant neutral fraction of gas. The amount of ionized gas in the filament system is estimated to be of order 10^5–10^7 $M_\odot$. If the filaments are overpressured with respect to the coronal gas, and fully ionized, e.g., if they are evaporating debris, or if there is a large neutral fraction then the dust-to-gas ratio is closer to the Galactic value.

The apparent outflow near the nucleus may be a small-scale galactic wind within which the cooler 10^4 K material is entrained, or it may be due to the dynamical influence of the synchrotron jet. The capture of a small, dusty gas-rich dwarf may have occurred which has triggered the current activity, and whose gaseous remnant now forms the emission filament/dust system. If the filaments have condensed from the coronal phase in a cooling flow, then the cooling must have proceeded to a point where dust has been able to form.

Subject headings: galaxies: individual (M87) — galaxies: interactions — galaxies: ISM

1. INTRODUCTION

The relative proximity of M87 ($D = 14.7 \pm 1$ Mpc; Jacoby, Ciardullo, & Ford 1990), its central location in the nearest X-ray emitting cluster of galaxies, the Virgo cluster, and the prominence of nonthermal emission seen from radio to X-ray wavelengths, in particular the well-known jet (Biretta, Stern, & Harris 1991), have resulted in numerous detailed studies of the galaxy, its environment, and associated nuclear activity. Here, we investigate a component of the M87 system—the extended, low-excitation, optical-line-emitting gas—which may link galactic processes such as the evolution of the interstellar medium and the relationship between optical and X-ray emitting plasma, to nonthermal nuclear processes that are ultimately responsible for the generation of the jet and lobes of powerful radio emission. The presence of optical line emission which arises from gas at temperature $\sim 10^4$ K may be indicative of a recent tidal accretion or capture event (Sparks 1992), which in turn may be responsible for the onset of the activity, or it may be symptomatic of the thermal instability within the hot $\sim 10^7$ K coronal gas known to pervade the galaxy and cluster (Ford & Butcher 1979; Stewart et al. 1984). The presence of similar low-excitation, extended optical line emission has been established in a significant fraction of elliptical galaxies using imaging through line-isolating filters (e.g., Heckman 1981; Baum et al. 1988; Heckman et al. 1989; Kim 1989; Sparks, Macchetto, & Golombek 1989; Forbes, Sparks, & Macchetto 1990; Trinchieri & di Serego Alighieri 1991; Macchetto & Sparks 1991), and through spectroscopic studies (e.g., Minkowski & Osterbrock 1950; Caldwell 1984; Phillips et al. 1986), hence the detailed analysis possible in the case of M87 offers the prospect of establishing an understanding of a phenomenon that is of quite wide generality.

Dust is often (perhaps always) found within the filament systems (Kim 1989; Machetto & Sparks 1991). This has implications for the origin and physical state of the material—dust must be able to form within it implying a significant, dense molecular fraction, or else the gas must in the past have been in an environment suitable for dust formation or injection. Observations of dust may also be used to constrain the geometry of the filament system. The covering factor may be inferred from the variation of extinction with wavelength, and the regions which lie in the foreground, and hence are seen in absorption against the background starlight, may also be identified.

In M87, extended filaments of Hα emission were discovered by Arp (1967) and studied in detail by Ford & Butcher (1979) who concluded that the most plausible origin for the line-emitting material is gas that has fallen into the nucleus, perhaps through thermal instability in the coronal plasma. Jarvis & Melnick (1991) and Jarvis & Peletier (1991) on the

[1] Based on observations collected at the National Optical Astronomy Observatories and at the European Southern Observatory, La Silla, Chile.

[2] Visiting Astronomer, Kitt Peak National Observatory, Operated by the Association of Universities for Research in Astronomy, Inc., under contract with the National Science Foundation.

other hand presented stellar spectroscopic observations that suggest a recent merger has occurred and that the nuclear velocity field betrays the presence of unrelaxed kinematic structure. Carter & Jenkins (1992) find the same result. Sparks (1992) discusses how such a merger, if the infalling galaxy is gas-rich, might influence the properties of the X-ray emitting coronal gas.

Here we present new imaging and emission-line spectroscopic observations that reveal the presence of dust associated with the emission filament system and show regularities in the velocity field. This places constraints on the origin of the line emitting gas and enables us to deduce a self-consistent picture of the approximate three-dimensional distribution of the gas with respect to the galaxy and hence to determine whether infall or outflow is occurring. Although we cannot resolve all ambiguities from the analysis with the present data, by different means we obtain a consistent picture whereby in the innermost region, outflow is apparent, but with infall at larger radii. We discuss how such a situation might arise and consider the energetics of the outflow.

2. OBSERVATIONS AND REDUCTIONS

2.1. *Monochromatic Images*

Narrow-band images of M87 were made at the f/2.77 prime focus of the KPNO 4 m telescope during 1985 April with the TI2 CCD binned 2 × 2 on-chip, giving an effective pixel size of 0.″6 and a 4′ × 4′ field. The Hα on-band filter was from KPNO Hα Filter Set A and had a nominal full width at half-maximum (FWHM) of 76 Å centered at $\lambda_c = 6606$ Å. The Hα off-band filter was centered at 6190 Å and had a FWHM of 347 Å.

The observations, summarized in Table 1, were made during photometric conditions and good seeing. The exposures centered on the nucleus were limited to 120 s in order to avoid overfilling the pixels from illumination by the strong nuclear continuum and emission.

The long exposures of Hα emission centered on a field 153″ south of the nucleus were contaminated by scattered light from a star near the edge of the field. Nonetheless, the images are suitable for showing the spatial structure in the faint, outermost filament.

The dc pedestal was removed from each CCD frame by subtracting the average of five zero-second exposures. Pixel-to-pixel and large-scale spatial variations in the sensitivity were corrected by dividing each frame by the average of five exposures of a white screen imaged through the corresponding filter.

Flux calibrations were derived by observing the stars Feige 34 and EG 129 through the Hα on-band filter. We derived the sensitivity function $S_{H\alpha}$ (ergs cm^{-2} count^{-1}) from the response of the standard stars, R_* (counts s^{-1}), by assuming the sensitivity and the absolute fluxes $F_{H\alpha,0}$ for Feige 34 (5.8×10^{-14} ergs cm^{-2} s^{-1}) and EG 129 (1.2×10^{-14} ergs cm^{-2} s^{-1}) are constant across the filter. $S_{H\alpha}$ is then given by the equation

$$S_{H\alpha} = F_{\lambda,0}\, e^{-\tau_{H\alpha,*}} A_{fil}\, R_*^{-1} . \quad (1)$$

The quantity $A_{fil} = \int_0^\infty T_\lambda\, d\lambda = 79.9$ Å was derived by integrating across the KPNO transmission curve of the filter. The atmospheric optical depth at Hα is given by $\tau_{H\alpha} = K_{H\alpha}$ (mag per air mass) X (air mass)/(2.5 $\log_{10} e$). We calculated $\tau_{H\alpha}$ by using the mean KPNO extinction coefficient $K_{6600} = 0.093$ mag per air mass taken from IRAF. The λ6606/76 filter transmits [N II] λ6548 ($T = 0.60$), Hα ($T = 0.85$), and [N II] λ6584 ($T = 0.84$). The relationship between the total intensity $I_{H\alpha+[N\,II]}$ (ergs cm^{-2} s^{-1} pixel^{-1}) and the Hα intensity is

$$I_{H\alpha+[N\,II]} = (1/3N + 1 + N) I_{H\alpha} , \quad (2)$$

where $N = 2.52$ is the average ratio of $I_{[N\,II]\lambda6584}$ to $I_{H\alpha}$ measured by Ford & Butcher (1979). The relationship between the total intensity and the observed count rate $R_{H\alpha+[N\,II]}$ is

$$I_{H\alpha+[N\,II]} = \frac{4.26}{3.41} R_{H\alpha+[N\,II]} S_{H\alpha} e^{\tau_{H\alpha}} . \quad (3)$$

2.2. *Monochromatic Intensities*

The strong underlying stellar continuum was removed from the on-band images by first taking the median of the on-band images and the median of the off-band images. Star positions were used to register the images. Then, the galaxy continuum in the off-band image was scaled to the on-band image and the off-band image was subtracted from the on-band image. The resulting Hα + [N II] image is shown in Figure 1.

The insets in Figure 1 (Plate 22) show the bright structure near the nucleus, and the outermost filament which is the sum of the two 1 hour exposures. The surface brightness $S_{H\alpha+[N\,II]}$ ergs cm^{-2} s^{-1} arcsec^{-2} is contoured quantitatively in Figure 2.

The total flux from the ionized gas was calculated by summing the intensities over 20 rectangular areas drawn

TABLE 1

M87 Hα OBSERVATIONS

Position	Filter λ_c/FWHM	Exposure Time (s)	Number of Exposures	Seeing
M87 Nucleus.....	6606/76	30	1	1.″0
M87 Nucleus.....	6606/76	120	5	1.0
M87 Nucleus.....	6190/347	30	6	1.0
Field 1	6606/76	3600	2	1.2
Field 1	6190/76	900	2	1.2

NOTE.—The long exposures for Hα emission centered on a field 153 south of the nucleus.

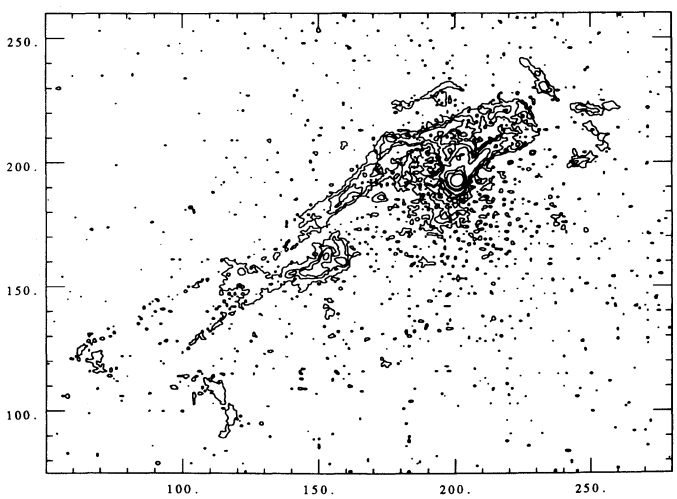

FIG. 2.—Contour map of the Hα + [N II] surface brightness. Levels are 1.5, 5, 10, 20, 50, 80, and 180 × 10^{-16} ergs s^{-1} cm^{-2} arcsec^{-2} with pixels 0.″6 on a side.

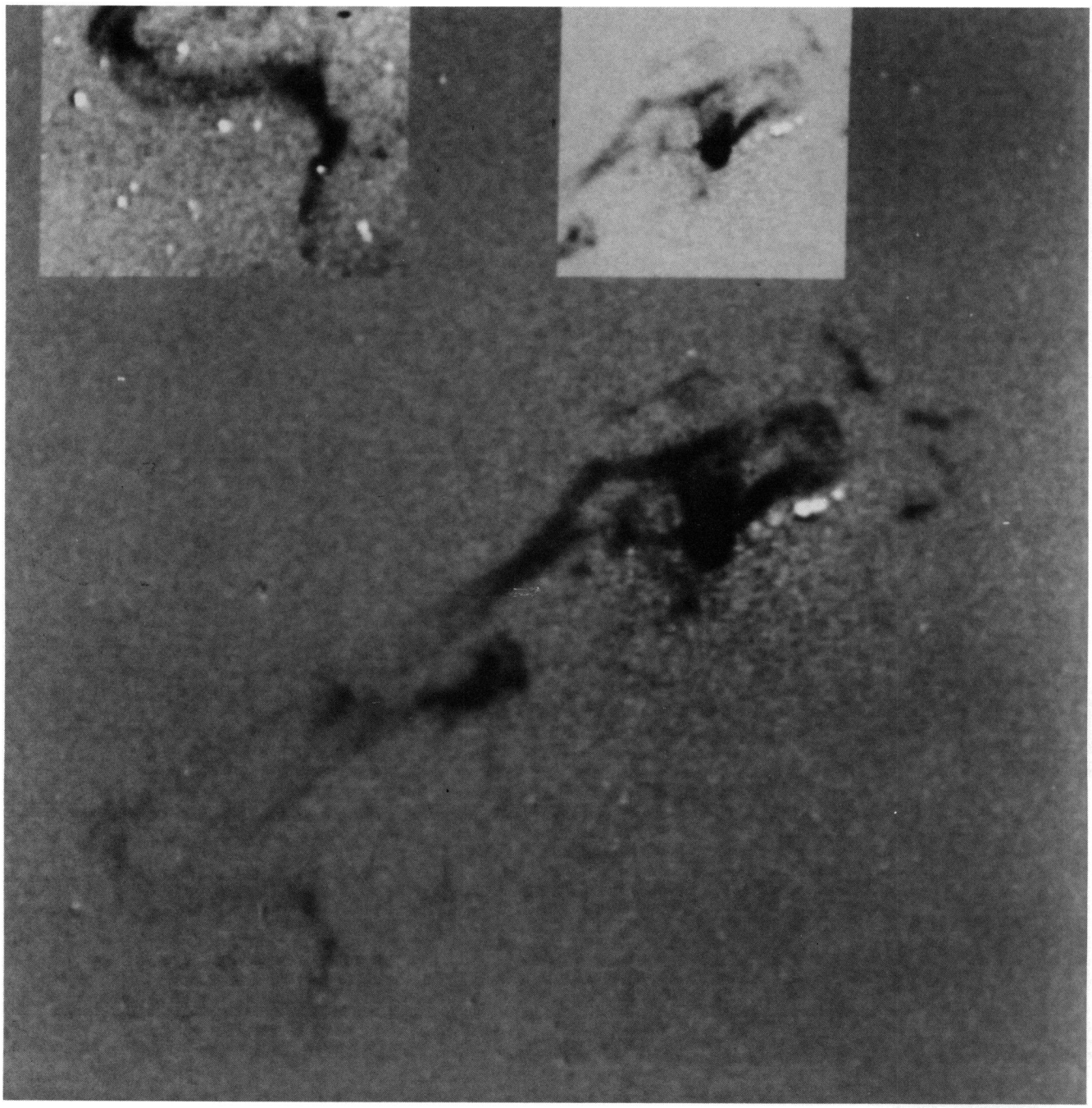

FIG. 1.—Hα + [N II] image of M87, the median of the on-band images after subtraction of a scaled median off-band continuum image. The insets at the top show the nuclear region on a different intensity scale, and the outer filament region at higher S/N from the "Field 1" observation. The total field of view is 2.'3 on a side, with north at the top.

SPARKS, FORD, & KINNEY (see 413, 532)

around the emission features seen in Figures 1 and 2. The residual sky level in each box was estimated from the sums in the adjacent boxes containing no discernable emission. Variation in the residual sky level introduced an uncertainty of $\sim 10\%$ in the flux from the faint outer filaments. The total flux is dominated by the bright center, where the residual sky level is negligible relative to the emission. The uncertainty in the total flux, which we estimate is 5% to 10%, is due to errors in the standard calibration, the mean extinction coefficient, and changes in the filter transmission. The total flux and the Hα flux are 1.18×10^{-12} and 2.8×10^{-13}, respectively, which for a distance of 14.7 Mpc translates to a total luminosity in Hα + [N II] $\approx 3 \times 10^{40}$ ergs s^{-1}. The limiting surface brightness is $\approx 0.5 \times 10^{-16}$ ergs s^{-1} cm^{-2} arcsec^{-2}, after slight smoothing. The total area covered by emission at a flux level above 10^{-16} ergs s^{-1} cm^{-2} arcsec^{-2} is ≈ 1250 arcsec^2. Figure 3 plots the radial distribution of surface brightness. The resulting flux maps are in good agreement with the data presented by Baum et al. (1988) and the total luminosities with Heckman et al. (1989).

2.3. *Continuum Imaging*

Direct continuum images of M87 were obtained using the ESO Faint Object Spectrograph and Camera (EFOSC) on the 3.6 m telescope at the European Southern Observatory 1990 February 22. The observations were a 2.5 minute V exposure, and V with neutral density polarizing filters, four minute exposures. The CCD used a high-resolution RCA thinned, back-illuminated chip, with 1024 × 640 pixels of side 0".34. The peak quantum efficiency was $\approx 70\%$ at around 5500 Å. The polarization properties are irrelevant for this work. In the areas of interest there was no significant difference between images taken through polarizers at different orientation. The polarizing filters have a throughput of $\approx 39\%$ for the unpolarized light as measured by observations of low-polarization photometric standard stars. An average zero exposure bias frame was subtracted from all images, and the images were flat-fielded by dividing the data by normalized exposures of a white screen inside the dome. In addition, we inspected V and R images obtained with the ESO New Technology Telescope (NTT) during 1990 April and described by Sparks et al. (1992). Each of these frames has an exposure time of 5 minutes with seeing $\approx 0".8$ FWHM and they were also taken with a thinned back-illuminated RCA CCD. Those data were also reduced in the standard fashion, using exposures of the twilight sky to flat-field the images. An absolute calibration was derived as discussed in Sparks et al. (1992) which included both the absolute zero point and an estimate of the sky level by comparison with the surface photometric profile of Young et al. (1978).

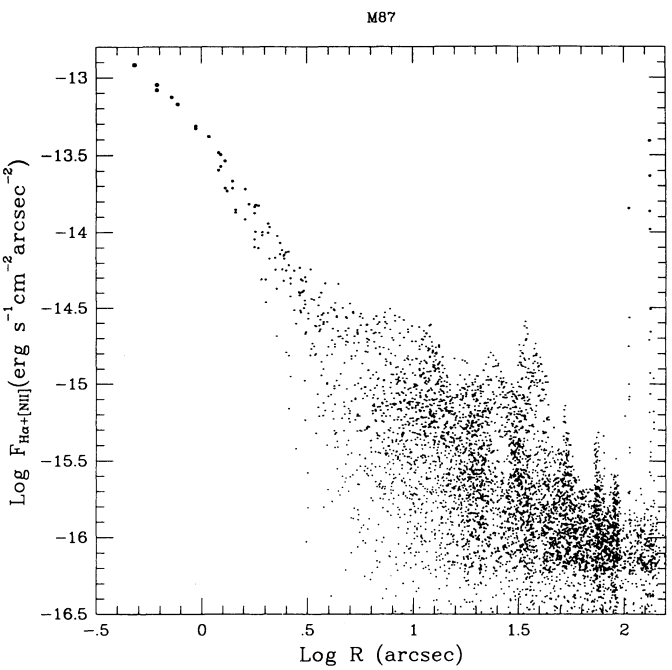

FIG. 3.—Surface brightnesses of individual pixels in ergs s^{-1} cm^{-2} arcsec^{-2} plotted against radius for the Hα + [N II] emission in M87.

A model of the smooth continuum stellar light distribution was generated by using ellipses fitted to isophotes, see Sparks et al. (1985) and Sparks, Laing, & Jenkins (1988). The region of the jet was masked out and a rejection algorithm applied to remove isophotal contour points greater than 2.5 σ from the mean radius. A model was then constructed to have purely elliptical isophotes, with the same parameters as the ellipses fitted to the galaxy data. An image of the dust optical depth within the galaxy was made by dividing the co-added V data by this model after sky subtraction (the sky level was estimated by comparing the surface brightness profile to the more extensive profile of Young et al. 1978). The resulting image was smoothed using a Gaussian of $\sigma = 1.0$ pixels to increase the S/N, and is displayed as Figure 4*a* (Plate 23). This image is the effective optical depth within the galaxy at each pixel, i.e., the fraction of light which is absorbed, with black corresponding to no absorption and white to absorption of 2% of the underlying continuum. Several patches of absorption are visible as described below in § 3.1. Figure 4*b* is an on-band Hα + [N II] image after subtraction of the model galaxy for comparison.

We emphasize that there is no ambiguity here—the absorption features are *deficits* of light compared to the model and cannot be induced artificially by the presence of line emission at the same locations. That is, we are witnessing directly the principal hallmark of dust, namely extinction. The jet cannot produce the apparent deficit through distortions of the ellipses fits, as shown in Sparks et al. (1988). There, it is clear that the inner dust patches are well separated from the jet and appear on only one side, which is inconsistent with ellipse distortion. For further confirmation, the dust absorption is clearly visible in the higher spatial resolution NTT images, shown in the galaxy-subtracted image of Sparks et al. (1992).

2.4. *Spectroscopic Observations and Reduction*

Spectra of the optical emission filaments were obtained during 1983 April with the RC spectrograph on the KPNO 4 m telescope. The detector was an RCA two-stage, magnetically focused image intensifier focused onto an 800 × 800 TI CCD (ICCD) with a transfer lens set to f/2.0. A 1200 lp/mm grating (B&L 380) blazed at 9000 Å in the first order was used with an RG1 blocking filter for the first order observations of Hα + [N II] and the [S II] lines. After 0.6 demagnification by the transfer lens, the spatial scale was 0".62 per pixel on the CCD, and the dispersion was 0.7 Å per pixel. The CCD was formatted to 480 × 536, giving 375 Å spectral range centered on 6637 Å. The slit width was 400 μm (2".6), giving a measured 2.2 Å FWHM. The observations are summarized in Table 2.

Initial reductions of the spectra were made at KPNO using

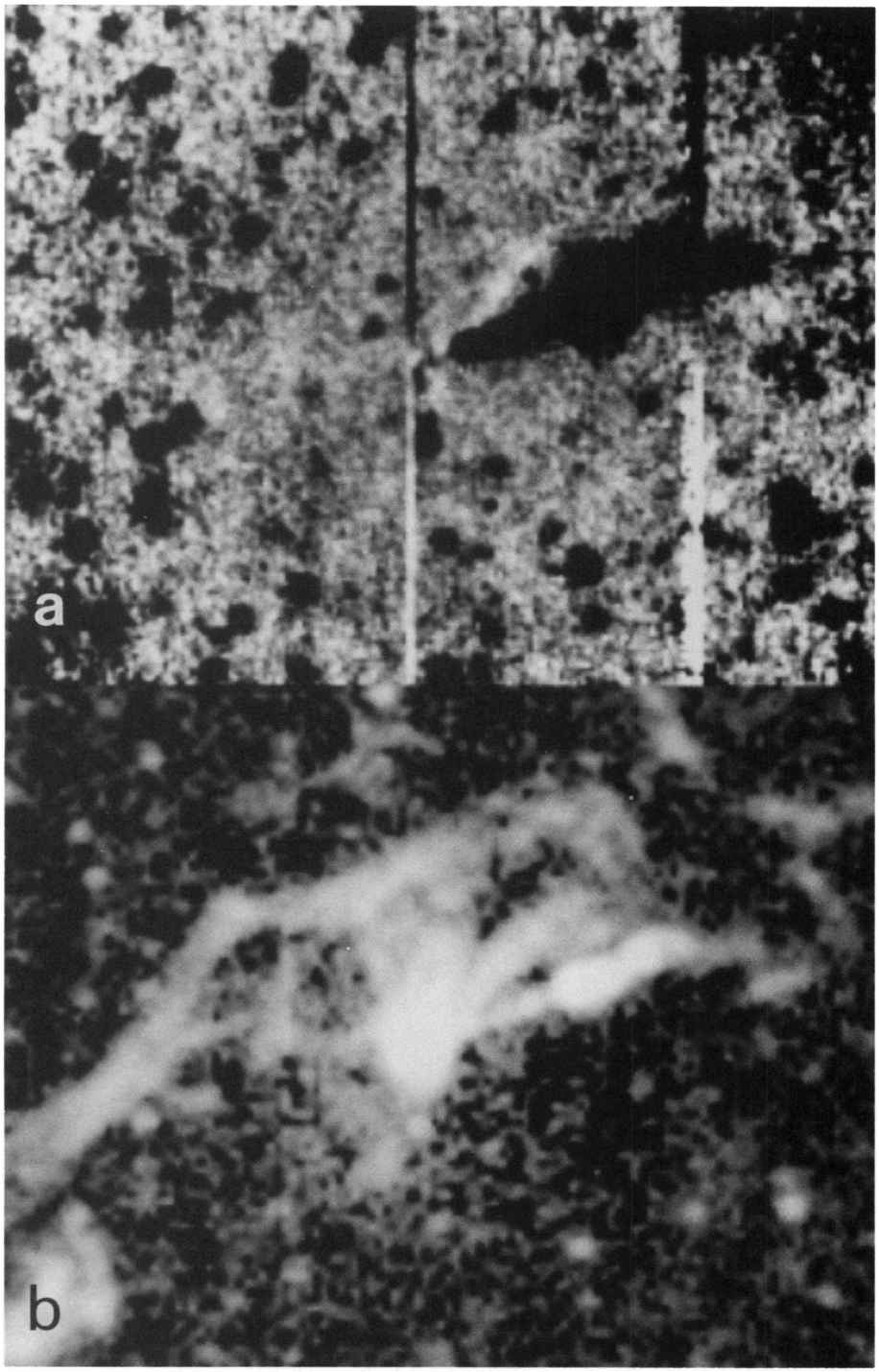

FIG. 4.—(*a*) Image of the optical depth in M87—ratio of continuum image to purely elliptical model of the galaxy, with patches of absorption shown as white. (*b*) On-band image after subtraction of the model galaxy for comparison.

SPARKS, FORD, & KINNEY (see 413, 533)

TABLE 2

SPECTROSCOPIC OBSERVATIONS OF M87, 1983 APRIL 13/14 AND 14/15

Spectrum	Offset From Nucleus	Position Angle	Exposure time (s)
P20	0".0	20°	1800
P105	11.2 E	105	2700
P111	0.0	111	1800
P125	0.0	125	1800
P133	0.0	133	3600
P150	19.5 E	150	2700
P174	0.0	174	1800

the Interactive Picture Processing System. Spectra of a quartz lamp and sky flats were used to remove high-frequency spatial variations in sensitivity and to flatten the spectra in the spatial direction. Neon comparison spectra were used to linearize the spectra in wavelength and in alignment along the column direction to ~0.1 pixel.

Final reductions and measurement of the radial velocities were made at STScI using NOAO IRAF programs. The spectra were relinearized to a starting wavelength of 6450 Å and a dispersion of 0.70 Å mm^{-1}. The rms residuals of the comparison lines were typically ~0.07 pixels. Because there was some flexure in the spectrograph and not all comparison spectra were taken immediately before and after the M87 spectra, a zero point correction was calculated for each spectrum by averaging the radial velocities of ~10 airglow lines. These average velocities are very well determined, with typical standard errors of ~2 km s^{-1}.

The airglow emission lines were removed from each spectrum by using the IRAF task "background" to fit fifth-order Legendre polynomial to each column above and below the rows containing emission from the filaments. The polynomials were then interpolated across the rows with emission and subtracted from them. The galaxy continuum was subtracted from each spectrum by fitting a fifth-order Legendre polynomial through the three segments of each row which did not contain emission from Hα + [N II] and [S II]. The polynomials were then interpolated across the emission line regions and subtracted from them. Figures 5 show the background-subtracted spectra reproduced at the same scale. The three emission lines on the left of each spectrum are [N II] λ6548, Hα 6563, and [N II] λ6584, and the doublet on the right of each spectrum is [S II] λ6716 and [S II] λ6731. All of the spectra which were centered on the nucleus show the well-known broadening of the emission lines in the nucleus (e.g., Osterbrock 1960).

2.5. *Measurement of Radial Velocities*

Before measuring radial velocities, each two-dimensional spectrum was sliced into a sequence of one-dimensional spectra by extracting and averaging three rows at a time. The radial velocities in each one-dimensional spectrum were measured by fitting Gaussian line profiles to [N II] λ6548.06, Hα 6562.813, and [N II] λ6583.39 (Bowen 1960). The observed velocities in each CCD frame were reduced to the solar rest frame by adding a heliocentric velocity correction and the zero-point shift determined from the average velocity of the airglow lines.

The internal consistency of the reductions and zero point corrections was estimated by comparing the velocities mea-

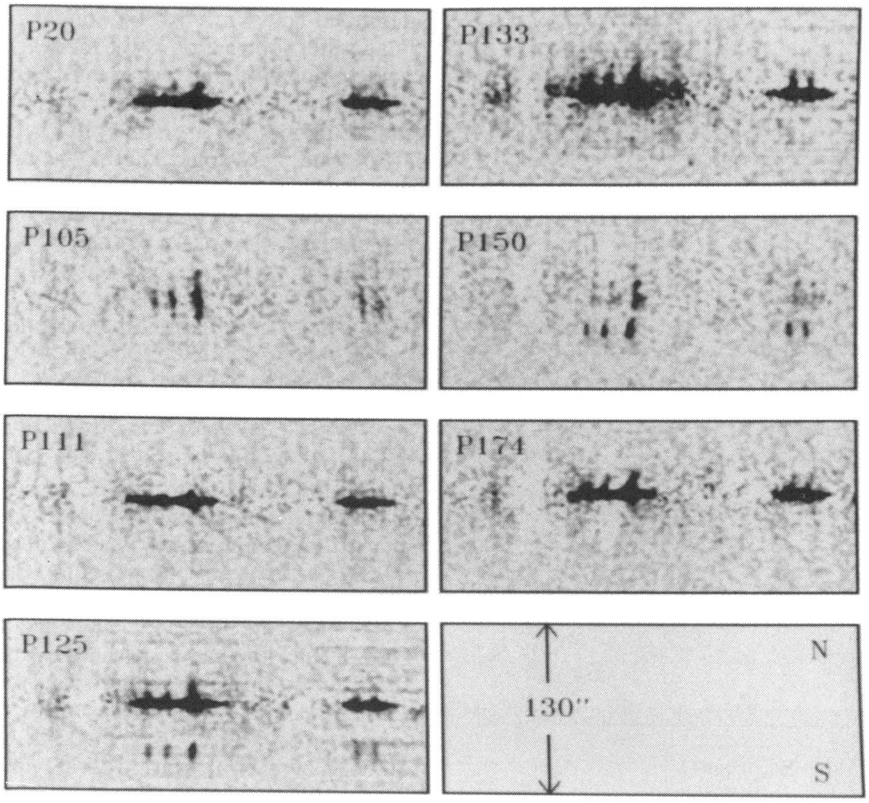

FIG. 5.—Background-subtracted spectra at each position angle on the same scale.

sured at similar positions near the nucleus in the spectra P125 and P133. This comparison shows that the internal accuracy is $\sim$5–10 km s^{-1}. A comparison betwen the velocities in this paper and those measured by Ford & Butcher (1979) shows that there is a marginally significant velocity difference of $\sim$20 km s^{-1} between the two data sets. Because the zero point in the present data has been set by the airglow lines in each spectrum, the velocities in this paper are likely to be more accurate than those given by Ford & Butcher (1979). We estimate that the accuracy of the projected positions along the slit direction is $\sim$1″–2″.

3. THE KILOPARSEC-SCALE INTERSTELLAR MATTER OF M87

3.1. *Morphology of Dust, Gas, and Radio Plasma*

The emission-line image is shown in Figure 1 and contoured in Figure 2. To facilitate comparison, the dust image in Figure 4*a* is shown adjacent to the emission-line image shown again in Figure 4*b*, but this time after subtraction of an elliptical model of the underlying continuum light distribution, rather than subtraction of a continuum image, so leaving globular clusters, etc., visible. Figure 4*b* has the same scale and orientation as Figure 4*a*. Note that in the image of the dust, the optical jet appears as a black feature, and the strongest contribution from dust, i.e., the brightest feature, comes from a region adjacent to and slightly north of the jet. This can be seen more clearly in Figure 6 which shows the data from the two images in Figure 4 overlaid in a contour map, with the optical line emission given as dotted contours and the absorption features as solid contours. Peak optical depths are typically $\tau \approx 0.02$, i.e., $\approx$2% of the light is extinguished by dust within the filaments. Note the close correspondence between the presence of optical line emission and absorption. Figure 7 (Plate 24) shows the relative locations of the optical line emission, shown in red, and nonthermal radiation as given by the radio emission, shown in cyan, with optical continuum (after underlying galaxy subtraction) as white. The radio image is the 6 cm 0.″4 resolution data of Hines, Owen, & Eilek (1989), by courtesy of F. Owen.

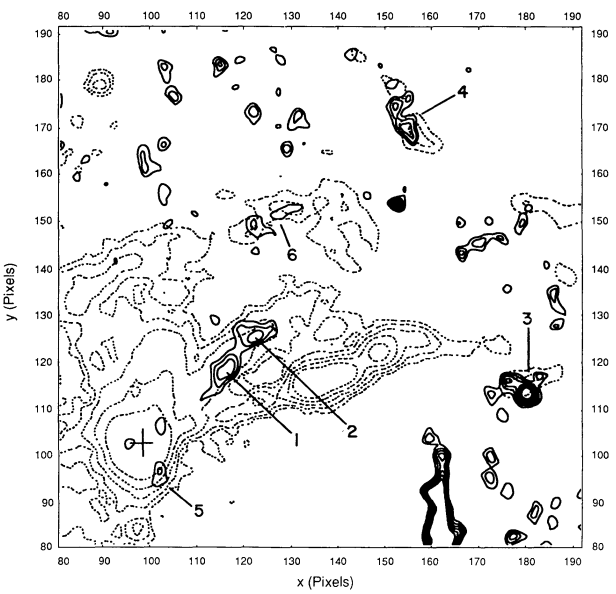

FIG. 6.—Contour map of the Hα + [N II] surface brightness and dust absorption patches, with particular features labeled for reference in the text. The data are those of Figs. 4*a* and 4*b* with solid contours the optical depth and dotted contours the model-subtracted on-band data.

The emission-line data (see also Fig. 1) show a bright radial feature extending in to the nucleus on the NW side (where the dust is), described by Jarvis (1991). A loop of emission is visible to the north (see insert in Fig. 1) and extends $\approx$8″ from the nucleus, and there is a diffuse "halo" within a few arcsec of the nucleus. Farther out, there are rather straight segments, two of which cross to the east of the nucleus and a brightening of the line emission occurs just beyond but very close to the SE radio lobe. At greater radial distances, there are large-scale loops and other "straight" segments. The filaments have a characteristic double-stranded structure, seen most clearly in these outer regions, but probably also present in the inner filaments. Such structure may arise from an edge-brightened cylindrical topology, or from an intrinsically "ribbon-like" topology. The presence of cross-overs favors a ribbon geometry; however, a more complex cylindrical geometry may be consistent if the bright rims are one-dimensional helical features on the surface of a cylinder. A third possibility is that they represent sheets, seen only where the sheets are close to edge on.

Patches of absorption are apparent running slightly to the north of the jet and close to it, labelled 1 and 2 in Figure 6. There is another patch $\approx$2″ southwest of the outermost tip of the jet, region 3, and also $\approx$14″ north of the jet, region 4. There is also a small patch of dust close to and south of the nucleus, region 5, and possibly two others labeled 6 in Figure 6. Additionally, the NTT image shows dust at a radius of 10″ in position angle 160° and another interior to "1" very close to the jet, at a radius 4.″5 in position angle 305°. Regions 1, 2, 3, and 5 are well above the S/N limit of the data, however regions 4 and 6 are close to the limits of the data. The inner feature (1–2) has been reported previously by Sparks et al. (1988), using a different data set.

The most prominent of the dust features—closest to the jet—are clearly coincident (in projection) with the brightest emission filament. In addition, the other dust patches are all exactly coincident with knots or filaments of line emission. This close association between dust and line emission, shown in Figure 6, is even more striking when seen on a display device with "blink" capability. While there are no places where dust is convincingly seen without line emission, the converse does not apply. For example, the SE quadrant of the galaxy has quite intense optical line emission with no associated absorption. The close association of dust and optical line emission is just what was found in the case of NGC 4696 by Sparks et al. (1989).

Turning to the radio data, there is a striking *anticorrelation* between the presence of line-emitting gas and radio-emitting plasma, Figure 7. The optical filaments all lie to one side of the radio emission. The emission filaments in particular avoid the SE lobe itself, yet are distributed closely around its edge, the brightest being where the filaments first encounter the outermost radio plasma. Interior to that point the Hα filaments can be traced throughout much of the image *except* wherever there is radio emission. There do not appear to be any strong correlations between optical line emission and the nonthermal jet. These results do not contradict the correlation found by Baum & Heckman (1989) where optical emission occurs preferentially in the radio emitting quadrants of radio galaxies, since that correlation applies only to powerful radio galaxies, the rarer Fanaroff-Riley Class II galaxies, although the overall axis of the optical emission is similar to that of the radio emission.

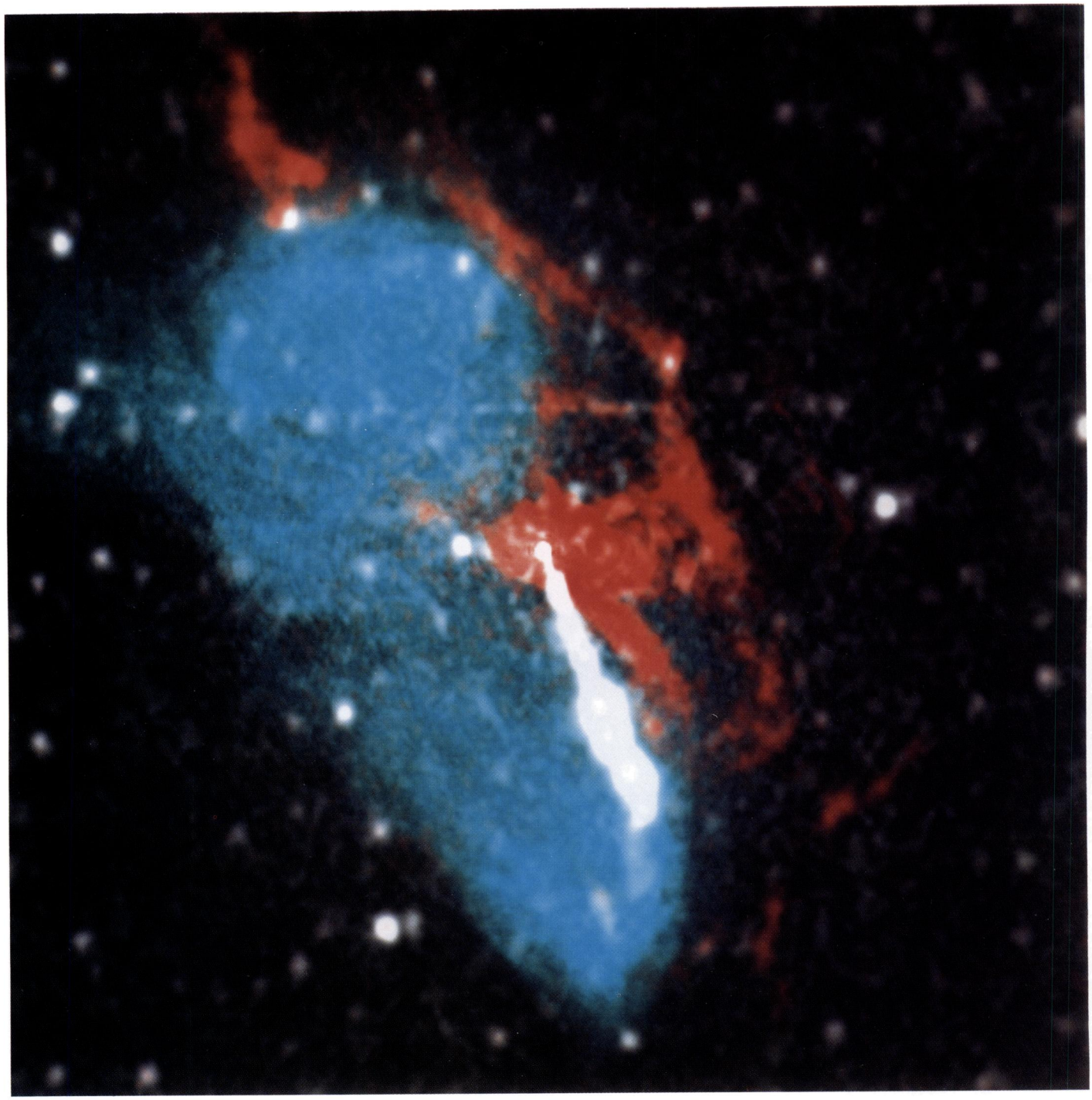

FIG. 7.—Composite image showing optical line emission in red, optical continuum in white (omitting the diffuse underlying elliptical galaxy light), and nonthermal radio emission in cyan, illustrating the avoidance of the inner radio lobes by the line-emitting material.

SPARKS, FORD, & KINNEY (see 413, 535)

M87 is more representative of radio luminous FR-I ellipticals and "cooling-flow" galaxies, with lower-level activity and non-thermal radiation confined within the optical extent of the galaxy. Baum & Heckman (1989) found no such correlation for these lower radio power galaxies. This was taken as evidence that more active galaxies photoionize the emission filaments, but that a different excitation mechanism may be needed in these less active objects.

3.2. *Geometry*

To attempt to determine the *geometry* of the system, we appeal to two aspects of the filament structure. Firstly, we see dust absorption which is direct evidence that the gaseous material is foreground to continuum light, and secondly radio observations indicate the SE lobe is background while the morphological connection between the optical and radio emission suggests that they are intrinsically close, in three dimensions, not just in projection.

To be more precise, weak absorption, $\tau \approx 0.02$, could arise from foreground material of low optical depth and high covering factor, from foreground material of high optical depth and low covering factor, or from background high optical depth, high covering factor material located at a distance such that it obscures 2% of the integrated line of sight. We can attempt to constrain this further by looking at the wavelength dependence of dust extinction. Sparks et al. (1989) presented an exact solution for the covering factor given measurement of extinction at two wavelengths, and in the Appendix, here, a likelihood solution to the same problem is presented. The latter is more appropriate to the low S/N available in the current case. Table 3 in the Appendix gives optical depths measured for three knots using the NTT V and R images. The maximum likelihood solution for the innermost two knots, which lie along the innermost radial filament, is that the covering factor is approximately one and the dust is entirely foreground. On the other hand, we cannot exclude, with any degree of statistical certainty, solutions which have the gas and dust lying up to 90% along the line of sight into the background, although to reiterate, the maximum-likelihood solution is that the dust lies in the foreground. Future higher S/N, high spatial resolution observations will resolve this ambiguity.

Next, we appeal to the close morphological relationship between the emission filament system and the radio lobes. The distribution of gas in the SE region suggests that it is intrinsically close to the SE radio lobe, rather than a random projection in the foreground of that lobe. Owen, Eilek, & Keel (1990) present Faraday rotation observations which indicate that the radiation of the SE lobe traverses a longer path length than the NW lobe, and they argue that this is most naturally understood if the SE lobe lies behind the galaxy and the Faraday rotation is due to the diffuse, magnetized ISM of the galaxy. Consistent with this view is that there is no absorption seen associated with the SE filaments. The presence of the jet itself on the NW side may add support to the proposition that it is foreground since relativistic beaming may be a factor in the apparent one-sidedness of the jet (Stiavelli et al. 1992; Sparks et al. 1992). This recent evidence for an active counterjet is consistent with the beaming concept. Owen, Hardee, & Cornwell (1989) also argue that the jet is foreground, although from its helical morphology, not very strongly inclined to the plane of the sky.

Thus, although the evidence is circumstantial, these observations do lead to an interesting, consistent picture in which the bright inner filament and the other NW side filaments are primarily foreground while the SE filaments lie in the background.

3.3. *The Velocity Field*

The velocity field for the line emitting gas is shown in Figures 8*a*, 8*b*, and 8*c*, after subtraction of the absorption-line systemic velocity of 1280 km s^{-1} (Huchra 1985). Negative is blueshifted with respect to the galaxy nucleus and positive is redshifted. Spectroscopically, we identify three regions. Moving out from the nucleus, the NW filament is *blueshifted* with respect to systemic velocity by $\approx$75 km s^{-1}. The tangential filament North of the nucleus at a distance of $\approx$12″ is *redshifted* by typically $\approx$150 km s^{-1}, and the bright filament beyond the SE radio lobe is again blueshifted by $\approx$100 km s^{-1}. Velocities up to a maximum of $\approx$430 km s^{-1} are seen, but with more typical magnitudes around 100 km s^{-1}, see also Figure 9 below.

Note that the NW side where velocities are primarily *blueshifted* is the side which from the discussion above is most likely to be in the *foreground*. That requires the gas to be on the nearside of the galaxy, moving toward us and therefore flowing out from the center. Conversely, around the SE lobe which is more distant from the nucleus and in the background, velocities are blueshifted and so infalling. The situation is ambiguous in the intermediate region where velocities are highest.

4. IMPLICATIONS AND DISCUSSION

4.1. *The Amount of Gas and Dust-to-Gas Ratio*

To summarize, the total flux in Hα + [N II] flux is 3×10^{40} ergs s^{-1}, and the total area covered by emission at a flux level above 10^{-16} ergs s^{-1} cm^{-2} arcsec^{-2} is $\approx$1250 arcsec^2. Energetically therefore, bearing in mind that the Hα + [N II] emission is expected to be a relatively small fraction of the total radiated flux (Heckman et al. 1989), the filament system is an important component of the interstellar medium in M87. The amount of *mass* in the filaments however is very small.

Firstly, consider to order of magnitude the implications of absorption. For a dust-to-gas ratio of d compared to the normal Galactic value, the corresponding gas column density N is

$$N(\mathrm{H}) \approx 1.9 \times 10^{21} A_V/d \ \mathrm{cm}^{-2} \qquad (4)$$

(Bohlin, Savage, & Drake 1978). Hence for $A_V \sim 0.01$ column densities of order 10^{19} cm^{-2} are required. Densities in the bright filaments are of order 200 cm^{-3} near the jet (Ford & Butcher 1979; Heckman et al. 1989), so if $N(\mathrm{H}) \approx n_e l$, for characteristic path length l, then $l \sim 0.03/d$ pc which is small compared to the transverse dimensions of the filaments and indicative of a low filling factor. For comparison, van Gorkom et al. (1989) found an H I absorption column density upper limit of 5×10^{19} cm^{-2}. If the whole filament system had a column density of order 10^{19} cm^{-2} then we would be dealing with $\sim 10^7 M_\odot$ of gas.

To proceed further, an estimate of the density is required. Schreier, Gorenstein, & Feigelson (1982) found a density in the coronal gas $n_e \approx 2/s$ cm^{-3}, where s is the radius in arcsec, and a temperature $T_e \approx 10^7$ K. We will adopt these values in order to estimate the pressure external to the filament system and assume the filament temperature is 10^4 K. The densities found by Ford & Butcher (1979) and Heckman et al. (1989) indicate that the filaments have pressure comparable to or somewhat

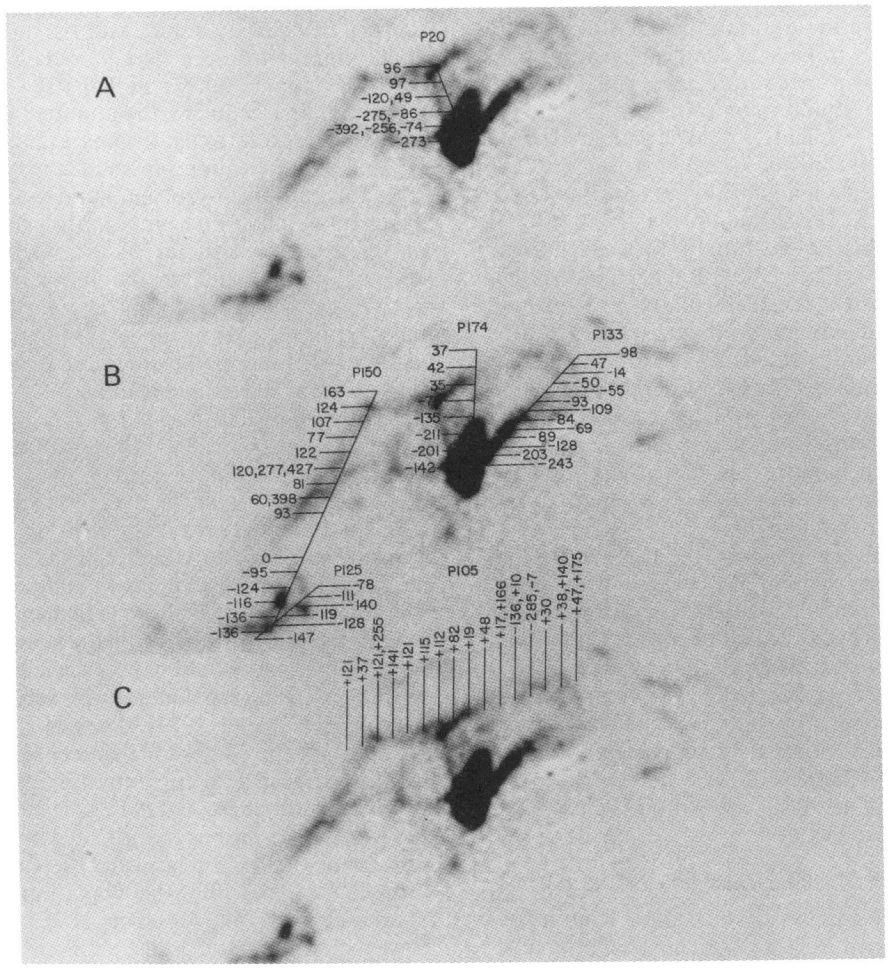

FIG. 8.—(*a*), (*b*), and (*c*) show the velocity field of emission-line material as derived from the long-slit spectroscopy, split into three diagrams to avoid confusion. A systemic component of 1280 km s^{-1} has been subtracted, and negative implies blueshifted, positive implies redshifted.

higher than this. Hence our estimate of the density is given by

$$2n_e + n_{\rm H} \approx 4000\zeta/(sp)\ , \tag{5}$$

where s is the projected radius in arcsec, p is the ratio of true to projected radius, and ζ is the amount by which the filaments are overpressured with respect to this simple model. The neutral gas density is $n_{\rm H}$. For gas at $T \approx 10^4$ K, the volume emissivity due to emission from Hα + [N II] is $\epsilon \approx 10^{-24} n_e^2$ ergs s^{-1} cm^{-3}. Converting this to observed surface brightness, F ergs s^{-1} cm^{-2} arcsec^{-2} we find

$$n_e^2\, l \approx n_e N({\rm H}^+) \approx 5.35 \times 10^{35} F({\rm H}\alpha + [{\rm N\ II}])\ , \tag{6}$$

where l as before is the path length, here in cm.

To estimate the amount of ionized gas, the ratio of equations (6) and (5) gives

$$N({\rm H}^+)\ {\rm cm}^{-2} \approx 0.389 s F_{16} \left(\frac{p}{\zeta}\right)\left(1 + \frac{f}{2}\right) \tag{7}$$

per 0.″6 pixel, where $f = n_{\rm H}/n_e$ (the neutral fraction) and F_{16} is the surface brightness in units of 10^{-16} ergs s^{-1} cm^{-2} arcsec^{-2}. Integrating the surface brightness data shown in Figure 3, this leads to a mass estimate in the range $M({\rm H}^+) \sim 0.5 \times 10^6$–$1 \times 10^7\ M_\odot$ assuming a typical $p \approx 2$ and f in the range 0 (fully ionized) to 40 (mostly neutral) and for pressure equilibrium. If the filaments have higher density than implied by pressure equilibrium, $\zeta > 1$ and the mass estimates are reduced inversely with ζ. Our final estimate of the ionized gas mass therefore is in the range 10^5–$10^7\ M_\odot$.

Although dust optical depths are small, it is of interest to determine whether the implied dust-to-gas ratio differs significantly from Galactic values. Combining equations (5) and (6) together with (8) which is equivalent to equation (4):

$$n_e\, l = 1.9 \times 10^{21} A_V/d(1+f) \tag{8}$$

we derive

$$(1+f)(2+f)\,\frac{pd}{\zeta} = 1.42 \times 10^{-11} A_V/(Fs) \tag{9}$$

where the right-hand side contains the observables, and the left the unknowns. $F \approx 1.35 \times 10^{-14}$ s$^{-1.18}$, is a power-law fit to the surface brightness data shown in Figure 3 (or else the values for regions 1 and 2 may be taken from Table 3). If the gas is fully ionized, $f = 0$, and typically, $pd/\zeta \approx 6$. So if the filaments are in front but close to their projected radius, $p \approx 2$, and in pressure equilibrium, $\zeta \approx 1$, the dust-to-gas ratio is about three times higher than a Galactic value. If the filaments are overpressured, the dust-to-gas ratio is even higher, by the overpressure factors. To get a Galactic value, $d = 1$, one option is to have the filaments significantly in the foreground, $p \approx 6$ or the angle from the nucleus to the dust patches of order 10° to

the line of sight. Another option to bring the dust-to-gas ratio down to a Galactic value is to have a significant neutral fraction, $f = n_H/n_e$. For modest projection factors, $p \approx 2$, normal dust-to-gas, and pressure equilibrium requires $f \approx 1.0$, i.e., $\sim 50\%$ ionization. If the filaments are overpressured by a factor 10, the required neutral factor is higher with $f \approx 6$. The implied column density for such a value of f is consistent with the limit of van Gorkom et al. (1989), but only just.

Suppose now that the dust-to-gas ratio is very much lower than the Galactic value, $d \approx 0.01$, Dwek, Rephaeli, & Mather (1990), which might happen if the filaments have condensed from a hot, dust-poor coronal phase. In that case, the required neutral fractions range from around 12 to 80 with higher values for higher overpressure. The equivalent H I column density is in excess of 3×10^{20} cm^{-2} which exceeds the observational limit mentioned. Simply put, we see enough dust that in order to have very much more gas than the equivalent amount of dust would imply in our Galaxy, we would violate the observed limit on the H I column density.

To hide the gas in a molecular phase, the gas density and mass would be much higher than for H I because of the much lower temperature. On the other hand, the observational upper limit for the molecular hydrogen content of M87 is rather high at present, $\sim 10^9 M_\odot$ (Lees et al. 1991). Carter & Jenkins (1992) have found evidence for a cool interstellar gas component in front of the nucleus, through observations of narrow optical absorption lines of calcium, although their required column densities are close to the H I limits.

It appears therefore that the dust-to-gas ratio is close to or higher than a normal Galactic value.

4.2. *Origin of the Dust*

If the cool emission-line gas has been accreted from a gas-rich dwarf, or tidally stripped from a gas-rich galaxy, the presence of dust is to be expected. A simple explanation for the large spatial extent but essentially coherent morphology which accounts for the presence of both gas and dust is that the gas and dust represents the debris of such infalling material—an immense "comet tail." This is consistent with the outer parts of the filament system, where we do indeed appear to see infalling material directly. The view that a recent merger has occurred within M87 has also been put forward by Jarvis & Peletier (1991) on the strength of stellar spectroscopic observations. In addition, a small merger may be responsible for triggering the nuclear activity, which in turn powers a modest outflow close to the nucleus. We return to this in § 4.3 where we discuss the circumstances under which the velocity field of the line-emission material may be influenced by the kinematics of the ambient hot gas.

Ford & Butcher (1979) on the other hand find an abnormally high nitrogen abundance in the filaments which is a potential difficulty for an infall model, and the spatial association of radio emission with optical line emission could be indicative of an alternative process. If the abundance of nitrogen is in fact normal, but the excitation mechanism is unusual, this may be overcome. Direct collisional heating of the filaments was proposed by Sparks et al. (1989) for NGC 4696, and is discussed as a possibility for the emission filaments of M87 by Sparks & Macchetto (1990) and Sparks (1992), while soft X-ray heating was shown by Voit & Donahue (1991) and Donahue & Voit (1991) to produce the characteristic nitrogen-strong LINER-type spectrum. Alternatively, if the filaments are in the process of evaporating due to their interaction (either thermal or hydrodynamic) with the ambient hot plasma, non-equilibrium ionization effects may be relevant (Ballet, Arnaud, & Rothenflug 1986); or perhaps the more volatile elements evaporate first, reducing the apparent abundance of hydrogen with respect to nitrogen. In any event, the strength of [N II]/Hα and its implication for abundances is a long-standing and (arguably) unsolved problem in the study of active nuclei. Also against an infall interpretation is the rough alignment of optical and radio structures—the outer regions of gas and dust are not perpendicular to the nonthermal "axis," contrary to what might be expected if the angular momentum of the gas is reflected in the axis of the jet. On the other hand, in a highly dissipative situation, the outer and innermost angular momentum axes may differ significantly.

Another possible origin for the gas and dust is residual material from inefficient heating of stellar ejecta to the temperatures of the diffuse coronal gas. A serious problem with this suggestion lies in the overall morphology of the emission filament system. There is no obvious reason why such stellar ejecta would adopt a roughly linear and highly coherent filamentary structure over many kiloparsecs.

A third possibility is that the filaments arise as condensation due to thermal instability of the coronal gas in a "cooling-flow." Here, one would expect such filaments to be dust-free since theoretical grain lifetimes are very short in the hot plasma (Draine & Salpeter 1979; Dwek et al. 1990). There are two potential escape routes for this scenario. First, the grains may be more robust than currently thought so that the dust *does* survive the hot phase. Dwek et al. (1990), however, showed that the *IRAS* observations of the Coma cluster imply a dust depletion factor of ~ 140 relative to the Galactic dust-to-gas ratio (referring to gas within the Coma intracluster medium). Also, Sparks et al. (1989) found in NGC 4696, in the Centaurus cluster, that the optical dust extinction as a function of wavelength is quite normal (consistent with Galactic dust). In that galaxy, which shows many similarities to M87, it therefore seems unlikely that the population of grains has been grossly modified, which is the minimum one would expect for dust survival in the coronal gas (Dwek et al. 1990). In M87, too, we have found a wavelength dependence of extinction consistent with the standard value (see Table 3 in the Appendix), and so robust dust grains seem unlikely to be the solution.

Alternatively, within the thermal instability model, grains may be produced during the cooling process. In order for grains to condense, the cooling gas must reach a cool, dense molecular phase with temperature ≈ 1000 K, e.g., Salpeter (1974, 1977). The observational upper limit on the molecular hydrogen content of M87 is only $\sim 10^9 M_\odot$ at present, Lees et al. (1991), which does not constrain that option significantly. Future more sensitive observations are required. Pressures within the central regions of M87 are likely to be comparable to those of giant molecular clouds in our own Galaxy. However, it is unclear whether grain growth does occur in that environment, and whether the grain population produced in such a manner would display the normal wavelength dependence of extinction.

A variant on the thermal instability model that requires further analysis invokes triggering of the instability by pressure increases within the coronal gas due to the interaction of the radio lobes and the ambient gas, and might, for example, explain why the optical filaments are so closely distributed around one side of the radio lobes. Given the high sound speeds within the coronal gas, a hydrodynamic perturbation

would seem unlikely to be effective, however, a more complex plasma instability cannot be excluded at this stage.

For dust to form in the envelopes of stars that themselves are formed in a hypothetical condensation process also seems unlikely. The most rapid evolution of massive stars still requires of order 10^7 yr, Maeder & Meynet (1989). After formation, stars and gas are kinematically decoupled, so a peculiar velocity of only ~ 50 km s^{-1} (less than the emission-line width, Heckman et al. 1989) would result in a drift of ~ 1 kpc in the lifetime of such a star, which is more than enough to carry it outside the filament system thereby making direct injection of dust into the filaments implausible. In any event we do not see any obvious star formation associated with the filaments and others have argued that in the high-pressure environment of a cooling-flow, preferentially *low*-mass stars would form that would take orders of magnitude longer to process material back into the gas phase (e.g., Fabian, Nulsen, & Canizares 1991). Also, the spectral character of the filament system is not that of a typical H II region photoionized by hot stars.

4.3. *Gas Motions, Dissipation, Outflow*

Could the velocity field simply reflect *rotation* of the emission-line gas within the gravitational field of M87? The change of sign of the velocity field associated with the disappearance of absorption is *not* what would be expected from rotation. For rotation, we expect all material on the same side of the apparent minor axis to have the same sign in velocity. This is not what is observed, and severe warping of the plane of rotation would be required.

Figure 9 shows the "rotation" velocity of M87 for two different models of the mass distribution: (i) a linear fit, by eye, to the large scale mass distribution as given by Fabricant & Gorenstein (1983) based on X-ray observations of M87; and (ii) by assuming a constant $M_V/L = 10.0$ (Richstone & Tremaine 1985), together with optical surface photometry inverted using Abel's integral equation (Young et al. 1978). The modulus of the observed velocities are also shown for comparison. Although subject to reduction by projection effects, the observed velocities show no relationship at all with either of the above models. Where the rotational velocity begins to decrease significantly, within 10″–20″ is where we observe a rising velocity with respect to the nucleus. Even the peak observed velocity is within the rotational velocity for either mass model, albeit only just so. In general the gas velocities appear to be too low to attribute to simple rotational motion about the nucleus. By the same token, velocities are also too low for simple freefall, unless we are particularly unlucky with orientation effects. Thus the magnitude of velocities in the emission filament system is indicative of a highly dissipative situation. If, for example, the filaments are close to pressure equilibrium with the coronal gas, this is to be expected.

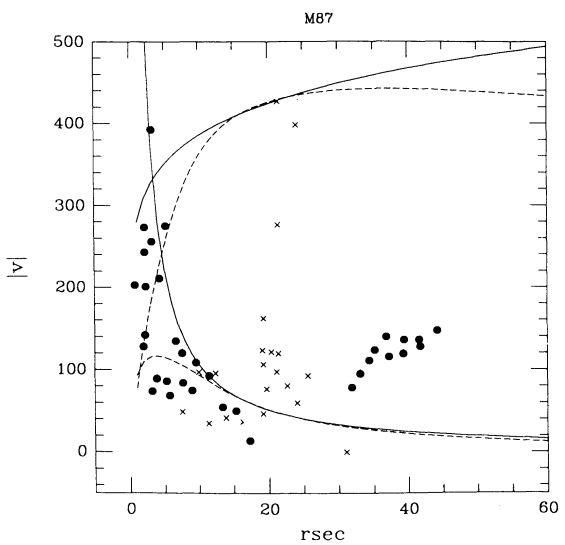

FIG. 9.—Observed absolute values of the radial velocities, solid symbols blueshifted with respect to systemic, crosses redshifted. Included for comparison are "rotation curves" (*upper pair*) and terminal velocity for an ionized cloud of mass 10 $M_\odot$ in pressure equilibrium with the coronal gas. Solid lines are for a mass distribution derived from Fabricant & Gorenstein (1983), and dashed lines are for constant M/L case with the luminosity profile of Young et al. (1978).

Since the filaments are immersed within the tenuous coronal gas, another characteristic velocity of interest is the terminal velocity of a test particle due to the viscous drag of the hot plasma. Using Spitzer's (1962) formula, $\mu = 2.21 \times 10^{-15} T^{5/2}/\ln\Lambda$ g cm^{-1} s^{-1}, the terminal velocity v_t (radial with respect to the nucleus) for a sphere of radius a, density ρ, at galactic radius and mass r and M immersed in plasma of viscosity μ is $v_t = \frac{2}{9} a^2 GM\rho/\mu r^2$ which results in the curves also shown in Figure 9 for a cloud of mass 10 $M_\odot$ at $T = 10^4$ K in pressure equilibrium with the halo. The tangential component of velocity would decay exponentially. Although characteristic terminal velocities are significantly closer to observed velocities, the sense of the motion is opposite to what would be expected from infall at the terminal speed. The point is to illustrate that for small clouds, the terminal velocity is lower than typical observed velocities. The terminal velocity scales with cloud mass to the power 2/3, so ionized clouds of mass less than or of order 10 $M_\odot$ are essentially brought to rest with respect to the halo gas by viscous forces. In such circumstances, their motion will echo the motions of the *hot* phase. The corresponding radius is of order 1 pc. We saw in § 4.2 that length scales within the filament system are indeed likely to be less than this. For topologies where the filament system comprises a "mist" of droplets such viscous effects are likely to be significant and the velocity field of the filaments will trace the velocity field of the hot phase. (Note that a low filling-factor mist does not exclude the high covering factor suggested by dust extinction.) Magnetic coupling between hot and cool phases would further enhance dissipation and link the kinematics of the two phases.

It is possible that the recent outburst of activity at the nucleus of M87, as evidenced by the presence of the optical synchrotron emitting jet and ongoing nuclear activity, with its consequent release of energy into the coronal gas, has caused a minor wind or "breeze" within that material, and that the filaments, trapped by viscous forces, move with the hot gas. A closely related picture is one in which the outwardly moving jet, seen to have proper motion typically ~ 0.2–$0.5c$, and up to $3.0c$ (Biretta & Owen 1993, in preparation) itself induces outflow in the hot phase to which the filaments may be coupled.

The kinetic energy of a spherical shell of radius r and thickness dr moving with velocity v is

$$dE = \tfrac{1}{2} 4\pi r^2 \, dr \rho v^2 \, . \tag{10}$$

For a distance of 14.7 Mpc, $\rho \approx 1.2 m_{\rm H} n_e$ and $n_e \approx 2/s$ with s the radius in arcsec, n_e in cm^{-3}, and expressing the velocity in units of 100 km s^{-1},

$$dE \approx 2.2 \times 10^{52} s v_{100}^2 \, ds \, . \tag{11}$$

To order of magnitude, if $v_{100} \approx 1$ and outflow occurs to a radius of 20″, then the total energy is $\sim 2 \times 10^{54}$ ergs. The kinetic energy of the filaments alone under similar assumptions in the outflowing region is about a factor 10 less than this. The sound speed in the coronal gas is ≈ 400 km s^{-1} and hence the sound crossing time for 20″ is 3.6×10^6 yr, which requires an energy input rate to the hot gas of order 2×10^{38} ergs s^{-1} to sustain such a wind. This may be compared to the nuclear luminosity of around 10^{41} ergs s^{-1} (νF_ν for a visual magnitude of 16.5), and it is clear that the energy transfer to the hot gas need only represent a small fraction of the total energy output of the nucleus.

4.4. *Magnetic Fields*

The linear, braided morphology of the optical emission filaments is strongly reminiscent of magnetically dominated structures, e.g., within the solar corona. Also, the Faraday rotation observations of Owen et al. (1990) show a filamentary nature and indicate a magnetic field whose strength may be dynamically important. Tribble (1989) has suggested a modification to the cooling flow theory of thermal instability in which magnetic confinement of the hot coronal plasma enables cooling to occur more rapidly. This is similar to the situation within the solar atmosphere, where Priest (1982) discusses the role of magnetic fields in shortening length scales in order that the thermal instability may occur and lead to prominence formation. The presence of dust in the optical filaments of M87 (and other "cooling-flows") however, must be accounted for by any successful theory relying on thermal instabilities to generate the filaments. As discussed above, perhaps dust can form within the condensing material once it has cooled below dust condensation temperatures of around 1000 K, Salpeter (1977), within a cold, dense molecular gas phase.

5. CONCLUSIONS

We have presented deep images of the extended, low-excitation, optical line emission in M87 and shown that the gas is filamentary in nature, with a double stranded morphology. We have shown that the ionized gas is dusty and that the wavelength dependence of extinction is consistent with a normal Galactic value. The velocity field of the emission line gas has been presented and the regularities within the kinematics identified. The optical emission avoids the inner radio lobes, although it is distributed closely around their periphery.

The dust-to-gas ratio is estimated to be quite close to a normal Galactic value, although, if anything, high compared to that norm. The quantity of gas involved in the filament system is estimated to be about 10^5–10^7 $M_\odot$. Several arguments indicate which regions of the gas and dust system are foreground, and which are background. This leads to a situation in which the gas and dust near the nucleus would be *outflowing* while the material farther out, beyond the SE radio lobe, is infalling.

A plausible explanation for the observed phenomena is that the capture of a small, dusty, gas-rich dwarf galaxy has occurred. The gaseous remains of the encounter now form the optical line emission system, and the velocity field of the optical gas echoes that of the hot, coronal gas. The merger has triggered the nuclear activity which in turn is powering the nonthermal jet and driving an outflow close to the nucleus. A rather modest kinetic energy transfer efficiency would be needed to achieve this. A more complete discussion of this possibility, together with other options may be found in § 4.

We thank Dave Lawrie for his efforts and assistance during the initial analysis of the spectroscopy. We also thank Andy Ptak for assistance in the processing of the direct imaging and Frazer Owen for providing the VLA radio image. Vera Rubin provided wavelengths for the airglow emission lines.

APPENDIX

A LIKELIHOOD SOLUTION TO THE EXTINCTION PROBLEM

In this Appendix we derive an expression for the "likelihood function," $z(\beta, \tau)$, describing how probable a given combination of intrinsic optical depth, τ, and fraction β of unreddened (foreground) light are for an observed pair of effective optical depth measurements at two different wavelengths, $s_{\rm obs0} \pm \sigma_0$ and $s_{\rm obs1} \pm \sigma_1$.

We suppose an absorbing cloud is spatially thin and lies at some distance along the line of sight of a distributed emission source, e.g., somewhere within the interior of a galaxy. If the "effective optical depth" (i.e., fraction of light extinguished) at wavelength λ_0 is s_0, then $s_0 = \beta + (1 - \beta)y$ where $y = e^{-\tau}$ measures the intrinsic optical depth of the cloud, then we define the function $z_0 = (s_0 - s_{\rm obs0})/\sigma_0$ which measures statistically how far from the observation a given model is, a model being specified by β and y (or equivalently τ). Clearly,

$$z_0 = [\beta + (1 - \beta)y - s_{\rm obs0}]/\sigma_0 \, . \tag{12}$$

Similarly, at wavelength λ_1, the fraction of unreddened light β is unchanged but the wavelength dependence of extinction fixes the optical depth at a different value, $y(\lambda_1) = y(\lambda_0)^\alpha$, such that the equivalent function

$$z_1 = [\beta + (1 - \beta)y^\alpha - s_{\rm obs1}]/\sigma_1 \, , \tag{13}$$

Then a general measure of the statistical quality of any given model for observed effective optical depths is

$$z(\beta, y) = \sqrt{\left[\frac{\beta + (1 - \beta)y - s_{\rm obs0}}{\sigma_0}\right]^2 + \left[\frac{\beta + (1 - \beta)y^\alpha - s_{\rm obs1}}{\sigma_1}\right]^2} \, . \tag{14}$$

The maximum likelihood solution is given by the minimum value of z—the β and y values of the minimum of z can be found numerically for a given pair of observations, $s_{\rm obs0} \pm \sigma_0$ and $s_{\rm obs1} \pm \sigma_1$. As might be expected, errors are highly correlated and rather than providing a simple well-isolated minimum, this method gives a locus of statistically acceptable solutions, where, as the optical depth goes up, so must the fraction of unreddened light to preserve the same effective extinctions.

TABLE 3

M87 EXTINCTION MEASUREMENTS

Region	s	θ	$F(\mathrm{H}\alpha + [\mathrm{N\ II}])$ (10^{-16} ergs s^{-1} cm^{-2} arcsec^{-2})	τ_V	τ_R	$z_{\min}$	$\beta_{\min}$	$\tau_{\min}$	Θ_{app}
1	8″	315°	25.1 ± 1.7	0.0173 ± 0.0015	0.008 ± 0.001	3.34	0.03	0.014	2.2 ± 0.3
2	11	314°	16.9 ± 1.2	0.0142 ± 0.0013	0.0095 ± 0.0009	0.59	0.01	0.014	1.5 ± 0.2
3	26	279°	6.5 ± 1.1	0.018 ± 0.002	0.015 ± 0.002	0.15	0.95	0.49	1.2 ± 0.2
C1				-0.0003 ± 0.0003	-0.0003 ± 0.0003				
C2				0.001 ± 0.001	0.002 ± 0.001				

Table 3 gives an example of measurements and associated maximum-likelihood values of τ and β for the NTT images, together with emission-line surface brightness measurements at the same locations for information. Θ_{app} is the apparent ratio of V to R extinction. The expected Galactic value is ≈ 1.3, hence departures from this value indicate either geometrical effects, as pursued within this Appendix, or grain size modification. Observed values are reasonably close to expected values and so this latter option is not pursued at this stage. Although the maximum likelihood solutions tend to lie at either extreme of the geometrical possibilities, the constraint is statistically rather weak as the value of z increases only slowly away from the minimum. Note that we do not have velocity information for region 3. The regions C1 and C2 are "control" regions close to the dust and emission filaments, but isolated from them.

REFERENCES

Arp, H. 1967, Astrophys. Lett., 1, 1
Ballet, J., Arnaud, M., & Rothenflug, R. 1986, A&A, 161, 12
Baum, S., & Heckman, T. 1989, ApJ, 336, 702
Baum, S., Heckman, T., Bridle, A., van Breugel, W., & Miley, G. 1988, ApJS, 68, 643
Biretta, J. A., Stern, C. P., & Harris, D. E. 1991, AJ, 101, 1632
Bohlin, R. C., Savage, B. D., & Drake, J. F. 1978, ApJ, 224, 132
Bowen, I. S. 1960, ApJ, 132, 1
Caldwell, N. 1984, PASP, 96, 287
Carter, D., & Jenkins, C. R. 1992, MNRAS, 257, 7P
Draine, B. T., & Salpeter, E. E. 1979, ApJ, 231, 77
Donahue, M., & Voit, G. M. 1991, ApJ, 381, 361
Dwek, E., Rephaeli, Y., & Mather, J. C. 1990, ApJ, 350, 104
Fabian, A. C., Nulsen, P. E. J., & Canizares, C. R. 1991, Astron. Astrophys. Rev., 2, 191
Fabricant, D., & Gorenstein, P. 1983, ApJ, 267, 535
Forbes, D. A., Sparks, W. B., & Macchetto, F. 1990, in IAU Colloq. 124, Paired and Interacting Galaxies, ed. J. W. Sulentic, W. C. Keel, & C. M. Telesco (NASA CP 3098), 431
Ford, H. C., & Butcher, H. 1979, ApJS, 41, 147
Heckman, T. M. 1981, ApJ, 250, L59
Heckman, T. M., Baum, S., van Breugel, W. J. M., & McCarthy, P. 1989, ApJ, 338, 48
Hines, D. C., Owen, F. N., & Eilek, J. A. 1980, ApJ, 347, 713
Huchra, J. P. 1985, in The Virgo Cluster of Galaxies, ed. A. Richter & B. Bingeli (Garching: ESO), 181
Jacoby, G. H., Ciardullo, R., & Ford, H. C. 1990, ApJ, 356, 332
Jarvis, B. J. 1991, A&A, 240, L8
Jarvis, B. J., & Melnick, J. 1991, A&A, 244, L1
Jarvis, B. J., & Peletier, R. F. 1991, A&A, 247, 315
Kim, D. 1989, ApJ, 346, 653
Lees, J. F., Knapp, G. R., Rupen, M. P., & Phillips, T. G. 1991, ApJ, 379, 177
Macchetto, F., & Sparks, W. B. 1991, in 5th OAC Internat. Workshop, Morphological and Physical Classification of Galaxies, ed. G. Longo, M. Capaccioli, & G. Busarello (Dordrecht: Kluwer), 191
Maeder, A., & Meynet, G. 1989, A&A, 210, 155
Minkowski, R., & Osterbrock, D. 1959, ApJ, 129, 583
Osterbrock, D. E. 1960, ApJ, 132, 325
Owen, F. N., Eilek, J. A., & Keel, W. C. 1990, ApJ, 362, 449
Owen, F. N., Hardee, P. E., & Cornwell, T. J. 1989, ApJ, 340, 698
Phillips, M. M., Jenkins, C. R., Dopita, M., Sadler, E., & Binette, L. 1986, AJ, 91, 1062
Priest, E. R. 1982, Solar Magnetohydrodynamics (Dordrecht: Reidel)
Richstone, D. D., & Tremaine, S. 1985, ApJ, 296, 370
Salpeter, E. E. 1974, ApJ, 193, 579
———. 1977, ARA&A, 15, 267
Schreier, E. J., Gorenstein, P., & Feigelson, E. D. 1982, ApJ, 261, 42
Sparks, W. B. 1992, ApJ, 399, 66
Sparks, W. B., Fraix-Burnet, D., Macchetto, F., & Owen, F. N. 1992, Nature, 355, 804
Sparks, W. B., Laing, R. A., & Jenkins, C. R. 1988, AJ, 95, 1684
Sparks, W. B., & Macchetto, F. 1990, in IAU Colloq. 124, Paired and Interacting Galaxies, ed. J. W. Sulentic, W. C. Keel, & C. M. Telesco (NASA CP 3098), 403
Sparks, W. B., Macchetto, F., & Golombek, D. 1989, ApJ, 345, 153
Sparks, W. B., Wall, J. V., Thorne, D. J., Jorden, P. R., van Breda, I. G., Rudd, P. J., & Jørgensen, H. E. 1985, MNRAS, 217, 87
Spitzer, L. 1962, Physics of Fully Ionized Gases (New York: Wiley)
Stewart, G. C., Canizares, C., Fabian, A. C., & Nulsen, P. E. J. 1984, ApJ, 278, 536
Stiavelli, M., Biretta, J., Møller, P., & Zeilinger, W. W. 1992, Nature, 355, 802
Tribble, P. C. 1989, MNRAS, 238, 1247
Trinchieri, G., & di Serego Alighieri, S. 1991, AJ, 101, 1647
van Gorkom, J. H., Knapp, G. R., Ekers, R. D., Ekers, D. D., Laing, R. A., & Polk, K. S. 1989, AJ, 97, 708
Voit, G. M., & Donahue, M. 1991, ApJ, 360, L15
Young, P. J., Westphal, J. A., Kristian, J., Wilson, C. P., & Landauer, F. P. 1978, ApJ, 221, 721